Decomposition and transposition model-matching technique in the absence of plane- of-array measurements and the evaluation of tilted solar collectors and their harvested solar resource

Keith de Souza

Decomposition and transposition model-matching technique in the absence of plane-of-array measurements and the evaluation of tilted solar collectors and their harvested solar resource

Cite as: J. Renewable Sustainable Energy **11**, 013701 (2019); https://doi.org/10.1063/1.5058115
Submitted: 17 September 2018 . Accepted: 24 December 2018 . Published Online: 14 January 2019

Keith De Souza

Journal of Renewable and Sustainable Energy ARTICLE scitation.org/journal/rse

Decomposition and transposition model-matching technique in the absence of plane-of-array measurements and the evaluation of tilted solar collectors and their harvested solar resource

Cite as: J. Renewable Sustainable Energy **11**, 013701 (2019); doi: 10.1063/1.5058115
Submitted: 17 September 2018 · Accepted: 24 December 2018 · Published Online: 14 January 2019

Keith De Souza

AFFILIATIONS

Center for Optoelectronics Research, Diego Martin, Trinidad and Tobago

ABSTRACT

Monthly optimum tilt angles of a flat-plate solar collector capable of south or north orientations were modeled for the tropical Caribbean island of Trinidad at 10.6° N latitude, using measured monthly average daily global and diffuse horizontal irradiation data from the period 2005–2010, as input to six transposition models comprising three isotropic (Liu and Jordan, Koronakis, and Badescu) and three anisotropic (Hay and Davies, 'Hay and Davies, Klucher and Reindl', and Ma and Iqbal) models. The anisotropic models were in good agreement with one another, and an easily implementable technique was devised to determine the best suited decomposition-transposition model matches from six decomposition models due to Liu and Jordan and Klein, Page, Collares-Perreira and Rabl, Iqbal, Erbs *et al.*, and Ibrahim. These matches can be used by territories having a similar climate to Trinidad but lacking measured diffuse horizontal irradiation or plane-of-array measurements, and the technique can be implemented globally by other host territories. The Ma and Iqbal model was chosen to simulate in detail the aforementioned collector as well as the one that was south-oriented only. A south/north-oriented collector required twelve monthly and two seasonal [April: 12.5° (north-oriented), October: 32° (south-oriented)], and annual [11.2° (south-oriented)] adjustments with corresponding gains in the collectable annual global solar irradiation compared to that on a horizontal surface of 9.3%, 7.9%, and 1.5%, respectively. In contrast, a south-oriented collector required eight monthly (September–April) and two seasonal (March: 0° and October: 35.5°) adjustments with lower corresponding gains of 7.6% and 7.1%, respectively.

I. INTRODUCTION

Solar energy is a renewable, pollution-free, and environmentally friendly resource that is freely available. When used as the fuel for solar energy based technologies, it leaves no carbon footprint. Investors, planners, designers, implementers, and users of these technologies, such as photovoltaic systems, require *a priori* quantitative assessment of the harvestable solar resource. A flat-plate solar collector such as a monofacial solar panel, which harnesses the solar irradiation to fuel these technologies, should be oriented and tilted optimally to capture maximum solar irradiation. This would mitigate against oversizing and increased costs of photovoltaic systems. However, solar resource assessments, if they exist at a given location, are usually quantified at most weather stations as global horizontal irradiation measured using pyranometers, and though valuable, does not represent the solar resource available to an optimally oriented and tilted flat-plate solar collector which is key to the performance evaluation of a photovoltaic system. To predict the total global solar irradiation (GSI) on such a collector (also known as the "plane-of-array" or "in-plane" GSI) from its corresponding horizontal solar irradiation, transposition models[1] are commonly used and have been in continual development spanning the last six decades.

If the goal is to assess the monthly average daily GSI on a tilted solar collector, then transposition models should ideally use the corresponding average inputs of the contemporaneously measured beam, diffuse, and global horizontal irradiation. At the minimum, they require the measured global horizontal irradiation, while the diffuse horizontal irradiation may be approximated using existing decomposition models[2–8] from which the beam irradiation may be approximated as the difference between the global and diffuse horizontal irradiation. If a

location has no measured horizontal irradiation, then the global component should be approximated by inputting available measured meteorological variables into appropriate existing empirical models. This study models the monthly average daily GSI on a tilted solar collector utilizing measured monthly average daily global and diffuse horizontal irradiation inputs.

Optimizing the collectable GSI of a flat-plate solar collector may be achieved by manual or automatic solar trackers;[9] the latter, particularly if dual-axis, is more expensive and more maintenance-intensive and requires electrical energy to operate which is usually derived from the harnessed solar energy. For the economies of some small-island states, manually optimizing the tilt angles of the collector on monthly, seasonal, or annual bases would be more economically feasible. In this paper, the collectable GSI of a flat-plate solar collector would be limited to monthly, seasonal, and annual adjustments of its tilt angles for south or north orientations, i.e., for surface azimuth angles of 0° or ±180°, respectively.

The motivation for this work was twofold: first, to study the performance of six transposition models in a climate that is tropical maritime and modified moist equatorial, characteristic of Trinidad, in order to simulate the aforementioned solar collectors, which is significant to the island's thrust and growth in the use of solar energy based technologies; second, to devise an easily implementable technique to determine the best performing decomposition-transposition model matches in a host territory in which measured diffuse horizontal irradiation data are available, which can then be used by other territories in which measured diffuse horizontal irradiation data are non-existent, but the climate is known to be similar to that of the host. In this way, rather than making an ad-hoc selection of decomposition and transposition models, which occurs widely in the literature, such territories would have access to a cadre of suitable matches that would allow a more accurate simulation of tilted solar collectors in the absence of comparative empirically determined tilt angles or plane-of-array GSI measurements.

The six transposition models selected for this study comprised three isotropic [Liu and Jordan (LJ)[10], Koronakis (K),[11] and Badescu (B)[12]] and three anisotropic [Hay and Davies (HD)[13],'Hay and Davies, Klucher and Reindl' (HDKR),[14,15] and Ma and Iqbal (MI)[16]] models. "HDKR" was coined by Duffie and Beckman[15] for a model developed by Reindl *et al.*,[14] who modified the Hay and Davies model with a term similar to that of Klucher[17]. Six decomposition models were considered and were due to Liu and Jordan[2] extended by Klein (LJK),[3] Page,[4] Collares-Perreira and Rabl (CPR),[5] Iqbal,[6] Erbs *et al.*,[7] and Ibrahim.[8] The transposition models were selected based on their global use, reported satisfactory performance and differences, while the decomposition models were selected primarily on the first two criteria.

The objectives of this paper are (i) to determine the monthly average daily global and diffuse horizontal irradiation from the measured data over the years 2005–2010, (ii) to assess the performance of the six transposition models for a tilted collector capable of south or north orientations, (iii) to determine the best decomposition-transposition model matches for the local and similar climates globally, and (iv) to select a suitable transposition model to comprehensively simulate and analyze tilted solar collectors in two modes of operation—south or north-oriented and south-oriented only—furnishing information that gives choice to investors, planners, designers, implementers, and users of solar based technologies and, in particular, photovoltaic systems for the tropical Caribbean island of Trinidad.

This paper is organized as follows. Section II provides a concise theory of fundamental equations and the transposition and decomposition models under consideration. Section III describes the methodology, and Sec. IV presents the results and discussion. Conclusions are given in Sec. V.

II. THEORY

Subsection II A provides the fundamental equations required. Subsection II B deals with the solar irradiation on a tilted solar collector and the six transposition models. Subsection II C provides the six decomposition models used to calculate monthly average daily diffuse horizontal irradiation from the corresponding global horizontal irradiation.

A. Fundamental equations

The daily extraterrestrial horizontal irradiation, H_o, in J m^{-2} day^{-1}, is given by[15]

$$H_0 = \left(\frac{86400 I_{sc}}{\pi}\right)\left[\cos\varphi\cos\delta\sin\omega_s + \left(\frac{\pi\omega_s}{180}\right)\sin\varphi\sin\delta\right] \times \left[1 + 0.033\cos\left(\frac{360\,x}{365}\right)\right], \quad (1)$$

where I_{sc} is the solar constant (1367 W/m^2), φ is the latitude of the location/weather station, δ is the sun declination angle, and ω_s is the sunset hour angle, all expressed in degrees. The following equations define δ[18] and ω_s[19] as:

$$\delta = 23.45\sin\left[360\,\frac{(284+x)}{365}\right], \quad -23.45^\circ \le \delta \le 23.45^\circ, \quad (2)$$

and

$$\omega_s = \cos^{-1}(-\tan\varphi\tan\delta), \quad (3)$$

where x is the day of the year in the Julian calendar, i.e., $1 \le x \le 365$; for example, $x = 1$ is for January 1st and $x = 365$ is for December 31st.

B. Solar irradiation on a tilted solar collector

The monthly average daily GSI on a tilted surface, $\overline{H}_{G,TILT}$, is the sum of three solar irradiation components incident on the surface and is given by

$$\overline{H}_{G,TILT} = \overline{H}_{B,TILT} + \overline{H}_{D,TILT} + \overline{H}_{R,TILT}, \quad (4)$$

where $\overline{H}_{B,TILT}$ is the beam solar irradiation on a tilted surface, $\overline{H}_{D,TILT}$ is the sky diffuse solar irradiation on a tilted surface, and $\overline{H}_{R,TILT}$ is the solar irradiation reflected from the ground diffusely and isotropically onto a tilted surface.

Similarly, the monthly average daily GSI on a horizontal surface, $\overline{H}_{G,HOR}$, is given by

$$\overline{H}_{G,HOR} = \overline{H}_{B,HOR} + \overline{H}_{D,HOR}, \quad (5)$$

where $\overline{H}_{B,HOR}$ and $\overline{H}_{D,HOR}$ are the corresponding beam and diffuse solar irradiation components, respectively. There is no component due to radiation reflected from the ground as in Eq. (4) since no ground reflections are incident on a horizontal surface. By rearrangement of Eq. (5), we obtain

$$\overline{H}_{B,HOR} = \overline{H}_{G,HOR} - \overline{H}_{D,HOR}, \tag{6}$$

and so, if the horizontal beam solar irradiation is not measured, it can be calculated provided that the global and diffuse horizontal irradiation is known.

Each of the tilt components on the right hand side of Eq. (4) can be expressed in terms of their corresponding horizontal components scaled by their tilt/conversion/transposition factors, R_b, R_d and R_s, thus giving

$$\overline{H}_{G,TILT} = \overline{H}_{B,HOR} R_b + \overline{H}_{D,HOR} R_d + \overline{H}_{G,HOR} \rho_g R_s, \tag{7}$$

where R_b and R_d are the ratios of the beam and diffuse solar irradiation on a tilted surface to their corresponding horizontal values, respectively, R_s is the tilt factor for the ground reflectance, and ρ_g is the ground's albedo or reflectance and assumes a value of[15,20] 0.2 in this study. Equation (7) is the general form of all transposition models, transposing horizontal components of irradiation to their tilted equivalents.

R_b, which is geometrically derived,[15,20] is the same for all transposition models and can be expressed as

$$R_b = \frac{\cos(\varphi \mp \beta)\cos\delta \sin\omega_{st} + \left(\frac{\pi}{180}\right)\omega_{st}\sin(\varphi \mp \beta)\sin\delta}{\cos\varphi\cos\delta\sin\omega_s + \left(\frac{\pi}{180}\right)\omega_s \sin\varphi\sin\delta}, \tag{8}$$

where all angles are in degrees. β is the tilt angle of the surface, i.e., the angle between the surface and the horizontal plane, and is defined in the range of $0^\circ \le \beta \le 180^\circ$, for a sloped surface of any orientation. Arguments $(\varphi - \beta)$ and $(\varphi + \beta)$ in Eq. (8) apply to a tilted surface facing true south and true north with the corresponding surface azimuth angles (measured from true south at 0°, negative due east, positive due west, and ±180° at true north) of 0° and ±180°, respectively. This explanation also applies to Eq. (9) below. ω_s, defined in Eq. (3), and ω_{st} are the sunset hour angle and the sunset hour angle for a tilted surface, respectively, for the average day of a month. ω_{st} is defined by

$$\omega_{st} = \min\begin{bmatrix} \cos^{-1}\left(-\tan(\varphi \mp \beta)\tan\delta\right) \\ \omega_s \end{bmatrix}, \tag{9}$$

where "min" means that ω_{st} takes the minimum of the two values calculated from the two expressions in the square brackets.

R_s is the same for most transposition models in the literature as for those in this study, but Badescu[12] defined it differently in his 3D approximation.

The main distinction between the transposition models however lies in their definitions of R_d furnished by the isotropic and anisotropic models' treatment of sky diffuse irradiation. Table I provides the expressions for R_d and R_s for the six transposition models in this study. Here, $A = \frac{(\overline{H}_{G,HOR} - \overline{H}_{D,HOR})}{\overline{H}_O}$, $f = \sqrt{\frac{(\overline{H}_{G,HOR} - \overline{H}_{D,HOR})}{\overline{H}_{G,HOR}}}$, and $\overline{K}_T = \frac{\overline{H}_{G,HOR}}{\overline{H}_O}$. A, the anisotropy index, gives the fraction of $\overline{H}_{D,HOR}$ that appears as circumsolar irradiation, while the remaining (1 − A) fraction accounts for the isotropic component. A correction factor, $\left(1 + f\sin^3(\beta/2)\right)$, accounts for horizon brightening where the modulation factor, f, accounts for clear sky and cloudy days. $\overline{K}_T$ is the monthly average daily clearness index.

TABLE I. Tilt factors, R_d and R_s, for the three isotropic (LJ, K, and B) and three anisotropic (HD, HDKR, and MI) transposition models.

Transposition model	R_d	R_s
Liu and Jordan (LJ)	$\left(\frac{1+\cos\beta}{2}\right)$	$\left(\frac{1-\cos\beta}{2}\right)$
Koronakis (K)	$\left(\frac{2+\cos\beta}{3}\right)$	$\left(\frac{1-\cos\beta}{2}\right)$
Badescu (B)	$\left(\frac{3+\cos 2\beta}{4}\right)$	$\left(\frac{1-\cos 2\beta}{4}\right)$
Hay and Davies (HD)	$AR_b + (1-A)\left(\frac{1+\cos\beta}{2}\right)$	$\left(\frac{1-\cos\beta}{2}\right)$
Hay and Davies, Klucher and Reindl (HDKR)	$AR_b + (1-A)\left(\frac{1+\cos\beta}{2}\right) \times \left(1 + f\sin^3\left(\frac{\beta}{2}\right)\right)$	$\left(\frac{1-\cos\beta}{2}\right)$
Ma and Iqbal (MI)	$\bar{K}_T R_b + (1-\bar{K}_T)\left(\frac{1+\cos\beta}{2}\right)$	$\left(\frac{1-\cos\beta}{2}\right)$

These models are described in detail in their original papers and in the abundant literature on the subject matter, and for brevity, they will not be expatiated upon. We will however highlight the differences in the models. For the isotropic models, the LJ and K models differ only in R_d. The B model differs from them in both R_d and R_s. The anisotropic models differ only in R_d, but they all depend on $\overline{K}_T$ since A can be expressed as $\overline{K}_T - \overline{H}_{D,HOR}/\overline{H}_O$. The HD and MI models consider sky diffuse irradiation as being composed of isotropic and circumsolar components and have similar forms of R_d, differing only in A and $\overline{K}_T$. The HDKR model includes the third component of sky diffuse irradiation—the horizon brightening component.

C. Decomposition models to estimate monthly average daily diffuse horizontal irradiation

Table II lists the six models used to estimate monthly average daily diffuse horizontal irradiation, the details of which can be obtained from their references. All the decomposition models depend on $\overline{K}_T$ and are therefore climate-dependent.

III. METHODOLOGY

The measured hourly global and diffuse horizontal irradiation data for the period 2005–2010 were obtained from the Trinidad and Tobago Meteorological Service which is located at 10 .59° N latitude, 61 .35° W longitude and 21.95 m above the mean sea level. The Trinidad and Tobago Meteorological Service, as a member of the World Meteorological Organization,

TABLE II. Decomposition models to estimate monthly average daily diffuse horizontal irradiation.

Model	Equation
LJK	$\bar{H}_{D,HOR} = \bar{H}_{G,HOR}\left(1.390 - 4.027\bar{K}_T + 5.531\bar{K}_T^{\,2} - 3.108\bar{K}_T^{\,3}\right)$
Page	$\bar{H}_{D,HOR} = \bar{H}_{G,HOR}\left(1.0 - 1.13\bar{K}_T\right)$
CPR	$\bar{H}_{D,HOR} = \bar{H}_{G,HOR}\left(\begin{matrix}0.775 + 0.00606(\omega_s - 90) \\ -[0.505 + 0.00455(\omega_s - 90)]\cos\left(115\bar{K}_T - 103\right)\end{matrix}\right)$
Iqbal	$\bar{H}_{D,HOR} = \bar{H}_{G,HOR}\left(0.958 - 0.982\bar{K}_T\right)$
Erbs *et al.*,	For $0.3 \le \bar{K}_T \le 0.8$ and $\omega_s \le 81.4^\circ$,
	$\bar{H}_{D,HOR} = \bar{H}_{G,HOR}\left(1.391 - 3.560\bar{K}_T + 4.189\bar{K}_T^{\,2} - 2.137\bar{K}_T^{\,3}\right)$
	For $\omega_s > 81.4^\circ$
	$\bar{H}_{D,HOR} = \bar{H}_{G,HOR}\left(1.311 - 3.022\bar{K}_T + 3.427\bar{K}_T^{\,2} - 1.821\bar{K}_T^{\,3}\right)$
Ibrahim	$\bar{H}_{D,HOR} = \bar{H}_{G,HOR}\left(0.636 - 0.279\bar{K}_T - 0.194\bar{K}_T^{\,2} - 0.383\bar{K}_T^{\,3}\right)$

follows the organization's standards and best practices with respect to the maintenance and calibration of its instruments.[21]

The hourly global horizontal irradiation dataset comprising 26 174 data points was subjected to quality control to determine whether there were any days where GSI exceeded the theoretically calculated extraterrestrial solar irradiation, which would have shown erroneous data. None were found. A complete dataset would have contained 28 470 data points. Therefore, 2296 data points were missing. The hourly diffuse horizontal irradiation data were also subjected to quality control by comparing their values with the corresponding values of hourly global horizontal irradiation. There were instances when the hourly diffuse horizontal irradiation exceeded the corresponding hourly global horizontal irradiation which signified egregious data. All such data were discarded. The quality-controlled hourly diffuse horizontal irradiation comprised 20 637 data points. Therefore, 7833 data points were missing.

Monthly average daily extraterrestrial horizontal irradiation was determined using Eq. (1). Measured monthly average daily global and diffuse horizontal irradiation was calculated from the hourly global and diffuse horizontal irradiation datasets for the period 2005–2010. Monthly average daily beam horizontal irradiation was calculated using Eq. (6). Plots of the monthly variation of the four types of monthly average daily horizontal irradiation were produced.

The monthly optimum tilt angles of a collector capable of south or north orientations were modelled by Eq. (7), using the measured monthly average daily global and diffuse horizontal irradiation as inputs to the six transposition models (LJ, K, B, HD, HDKR, and MI). For each month, the optimum tilt angle was determined using an in-house computer program which iteratively varied the tilt angle from 0° to 70° in steps of 0.1° while monitoring the GSI collected. The tilt angle at which the maximum GSI was collected was the optimum tilt angle for the month. The monthly optimum tilt angles for the beam irradiation were also calculated using Eq. (7), by ignoring the second and third terms. These tilt angles served as the baseline or reference angles, relative to which the monthly optimum tilt angles of the transposition models were compared and analyzed.

The monthly optimum tilt angles of the aforementioned collector were modelled by the transposition models by replacing the measured monthly average daily diffuse horizontal irradiation input with simulated monthly average daily diffuse horizontal irradiation from each of the six decomposition models (LJK, Page, CPR, Iqbal, Erbs *et al.*, and Ibrahim), in turn. Decomposition-transposition model matches were established by comparing the root mean square differences (RMSDs) between the monthly optimum tilt angles due to the decomposition models and those due to the measured monthly average daily diffuse horizontal irradiation.

Finally, a transposition model was selected to model monthly, seasonal, and annual optimum tilt angles for both the aforementioned solar collector and the one which was south-oriented only. For monthly, seasonal, and annual cases, the monthly and annually predicted tilted GSI was computed along with their corresponding percentage gains over the measured annual global horizontal irradiation. The annual tilted GSI of all six transposition models was computed and compared, and the percentage differences between the five unchosen models' GSI and that of the preferred model were determined.

IV. RESULTS AND DISCUSSION

Subsection IV A provides the necessary parameters for the average day of each month and quantifies the monthly average daily extraterrestrial, global, diffuse, and beam horizontal irradiation. Subsection IV B provides the monthly optimum tilt angles predicted by the six transposition models. Subsection IV C establishes the decomposition-transposition model matches. Subsection IV D analyzes in detail two solar collectors–one which is south or north-oriented during a year and another which is south-oriented only.

A. Monthly average daily horizontal irradiation

Table III shows the average day of each month as recommended by Klein[3] and the calculated values of δ from Eq. (2). Figure 1(a) shows the variation of the monthly average daily extraterrestrial, global, beam, and diffuse horizontal irradiation over the six-year period 2005–2010. The global and diffuse solar

TABLE III. Recommended average day of each month, day number, and δ.

Month and	day	Day number	δ (degrees)
Jan	17	17	−20.92
Feb	16	47	−12.95
Mar	16	75	−2.42
Apr	15	105	9.41
May	15	135	18.79
Jun	11	162	23.09
Jul	17	198	21.18
Aug	16	228	13.45
Sep	15	258	2.22
Oct	15	288	−9.60
Nov	14	318	−18.91
Dec	10	344	−23.05

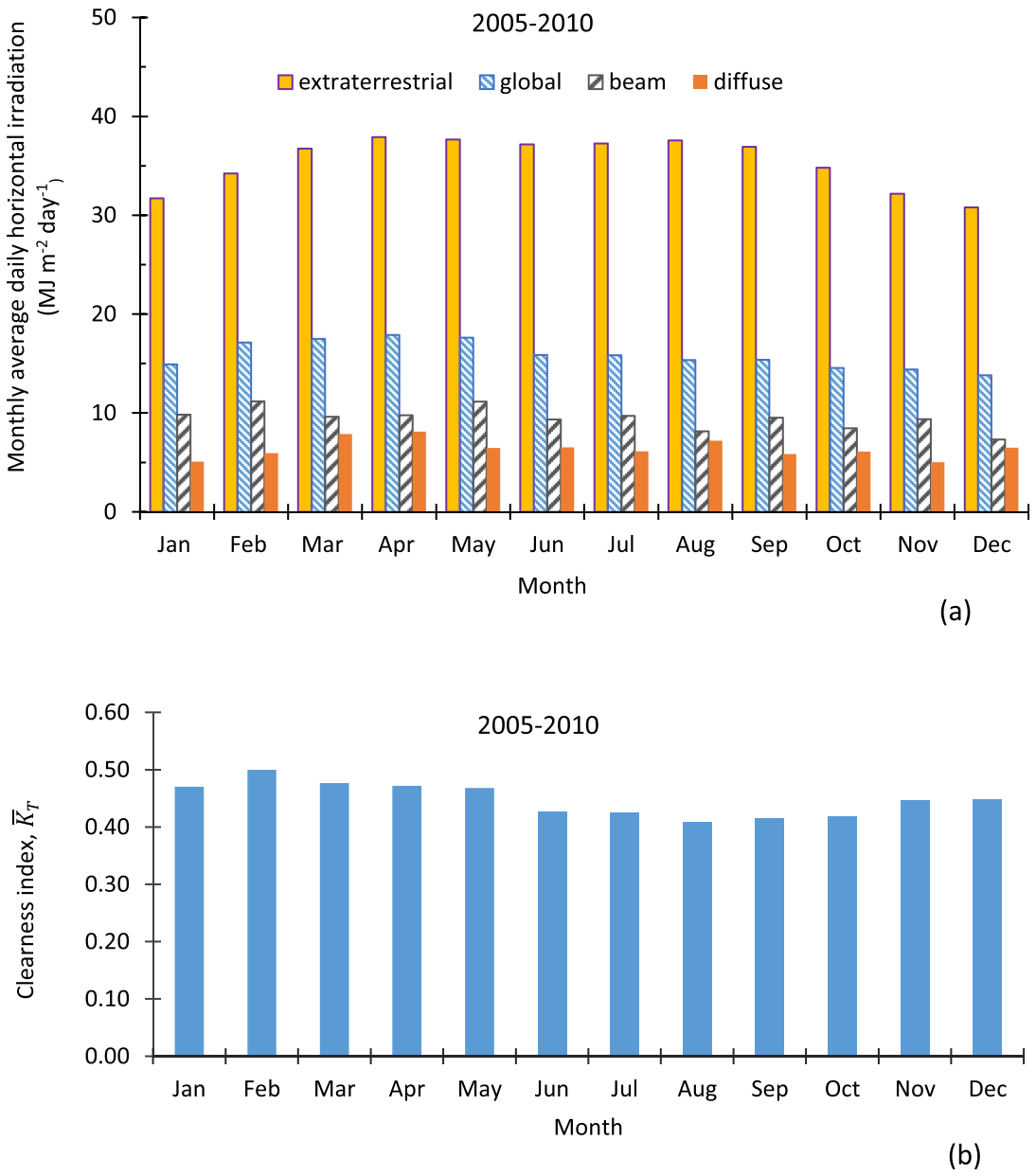

FIG. 1. Variation of the monthly average daily (a) extraterrestrial, global, beam, and diffuse horizontal irradiation over the six-year period 2005–2010 where the global and diffuse irradiation was measured and the extraterrestrial and beam irradiation was calculated and (b) clearness index.

irradiation was measured, while the extraterrestrial and beam horizontal irradiation was calculated using Eqs. (1) and (6), respectively.

The extraterrestrial horizontal irradiation has minimum values of 31.7 and 30.8 MJ $m^{-2}day^{-1}$ in January and December, respectively, a local minimum of 37.2 MJ $m^{-2}day^{-1}$ in June, and local maxima values of 37.9 and 37.6 MJ $m^{-2}day^{-1}$ in April and August, respectively. The global horizontal irradiation has minimum values of 14.9 and 13.8 MJ $m^{-2}day^{-1}$ in January and December, respectively, and a maximum value of 17.9 MJ $m^{-2}day^{-1}$ in April. The global horizontal irradiation has minimum values of 14.9 and 13.8 MJ $m^{-2}day^{-1}$ in January and December, respectively, and a maximum value of 17.9 MJ $m^{-2}day^{-1}$ in April. The beam horizontal irradiation has minimum and maximum values of 13.8 and 17.9 MJ $m^{-2}day^{-1}$ in December and April, respectively. The diffuse horizontal irradiation has minimum and maximum values of 5.0 and 8.1 MJ $m^{-2}day^{-1}$ in November and April, respectively. It should be noted that the

beam horizontal irradiation always exceeds the diffuse horizontal irradiation, thereby showing its dominance for typical days of every month.

Figure 1(b) shows the monthly average daily clearness index, $\overline{K}_T$, where $0.41 \leq \overline{K}_T \leq 0.50$ with a minimum of 0.41 in August, a maximum of 0.5 in February, and average values of 0.48 and 0.43 for the dry (January–May) and wet (June–December) seasons, respectively. The sky conditions for the typical days of the months during a year can thus be classified as intermediate or partly cloudy[22–24] on which basis one can reasonably deduce that a transposition model that assumes pure or near-isotropic diffuse irradiation conditions (consistent with overcast or near-overcast conditions) would not be accurate for Trinidad as it does not reflect the inherent meteorological conditions of typical days.

B. Monthly optimum tilt angles for the six transposition models

Figure 2 shows the variation of the monthly optimum tilt angles for the six transposition models and the beam irradiation only—the former plotted as lines and the latter as point plots for the sake of clarity. For the local latitude, the collector should be south-oriented from September to March and north-oriented from April to August in order to maximize the monthly collected GSI since the sun's trajectory across the sky dome is south of the east-west line or line of latitude of the solar collector from September to March between sunrise and sunset and predominantly north of the east-west line from April to August. Recall that by definition, $0^\circ \leq \beta \leq 180^\circ$ for a sloped surface of any orientation. The negative values shown for the tilt angles are for convenience in separating the south-oriented months from the north-oriented months; it is $|\beta_{opt}|$ that is important. It should be noted that the tilt angles for the beam irradiation are independent of the amount of beam irradiation as they are derived from purely geometric considerations. These tilt angles can therefore serve as baseline or reference angles about which the corresponding angles from the transposition models fluctuate. The isotropic diffuse irradiation would tend to decrease the tilt angle below the reference angle, while the ground-reflected irradiation would tend to increase it; its final optimum value depends on the magnitudes of the relative changes among the three solar irradiation components harvested by the collector. Thus, if the tilt angle of the collector is decreased below the reference angle and the increase in collected isotropic diffuse irradiation exceeds the corresponding decrease in the sum of the collected beam (and circumsolar if applicable) and ground-reflected irradiation, then the optimum tilt angle (when the increase equals the decrease) would be less than the reference angle. Conversely, if the tilt angle of the collector is increased above the reference angle and the increase in collected ground-reflected irradiation exceeds the decrease in the sum of the collected beam (and circumsolar if applicable) and isotropic diffuse irradiation, then the optimum tilt angle would be greater than the reference angle.

The isotropic LJ and B models are easily distinguishable in the graph, while the isotropic K and anisotropic HD, HDKR, and MI models are less so, predicting close monthly optimum tilt angles, especially the MI and HDKR models. The K model's tilt angles are close to those of the HD model. It is clear that the K, HD, HDKR, and MI models' monthly optimum tilt angles are in relatively close agreement with the reference angles (point plots), while the LJ and B models are skewed further away from them. This indicates that the anisotropic models assign greater relative importance to the beam and co-propagating circumsolar diffuse components than to the isotropic diffuse component of the solar irradiation, while the LJ and B models (with zero circumsolar component) reduce and increase the weighting of these respective components per Eq. (7). Interestingly, the

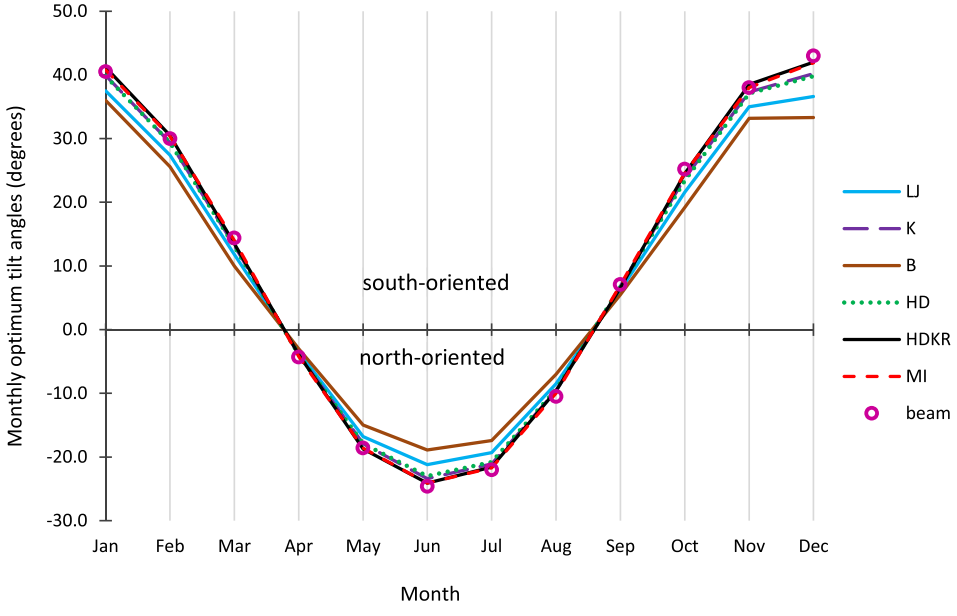

FIG. 2. The monthly optimum tilt angles of the six transposition models (lines) and the beam irradiation (points) for a solar collector capable of south or north orientations.

TABLE IV. *RMSD* (°) between the monthly optimum tilt angles from each of the six transposition models and the reference angles.

Transposition models	LJ	K	B	HD	HDKR	MI
RMSD(°)	3.07	1.16	4.96	1.38	0.64	0.46

pseudo-isotropic nature of the K model aligns itself closer to the anisotropic models for the local climatological conditions, while the pseudo-isotropic nature of the B model does not.

Quantification of the closeness of the transposition models' monthly optimum tilt angles to the reference angles is given by the *RMSDs* in Table IV. The *RMSD* (°) was calculated using

$$\mathrm{RMSD}(^\circ) = \left[\frac{1}{n}\sum_{i=1}^{n}\left(\beta_{opt,j,meas} - \beta_{opt,ref}\right)^2\right]^{1/2}, \quad (10)$$

where n is the number of months in a year = 12, $\beta_{opt,j,meas}$ are the monthly optimum tilt angles predicted by the transposition model, j = LJ, K, B, HD, HDKR, or MI using the measured monthly average daily diffuse horizontal irradiation data, and $\beta_{opt,ref}$ are the corresponding monthly optimum tilt angles (reference angles) of the beam irradiation. The HDKR and MI models are within 1° *RMSD* from the reference tilt angles, which indicates that the monthly optimum tilt angles computed from the beam irradiation only are very good estimates of the HDKR and MI's tilt angles.

C. Establishing the decomposition-transposition model matches

Table V shows the MI transposition model's predicted monthly optimum tilt angles due to the decomposition models and the measured diffuse horizontal irradiation, along with the calculated *RMSD* values. Similar tables were composed for the other five transposition models.

Similar to Eq. (10), the *RMSD* (°) was calculated using

TABLE V. Monthly optimum tilt angles (degrees) from the MI transposition model using measured monthly average daily diffuse horizontal irradiation and simulated diffuse horizontal irradiation from the six decomposition models. Emboldened angles are for a north-oriented collector, otherwise south-oriented. The values of *RMSD* (°) are shown.

Month	LJK	Page	CPR	Iqbal	Erbs *et al.*,	Ibrahim	Measured
Jan	40.3	39.6	40.0	39.3	39.7	40.1	40.8
Feb	30.2	29.7	29.9	29.4	29.7	30.0	30.4
Mar	14.3	14.0	14.1	13.9	14.0	14.2	14.0
Apr	**4.3**	**4.2**	**4.2**	**4.1**	**4.2**	**4.2**	**4.2**
May	**18.4**	**18.0**	**18.1**	**17.8**	**18.1**	**18.3**	**18.6**
Jun	**23.9**	**23.2**	**23.5**	**23.0**	**23.4**	**23.8**	**24.1**
Jul	**21.3**	**20.7**	**20.9**	**20.5**	**20.8**	**21.2**	**21.7**
Aug	**10.1**	**9.8**	**9.9**	**9.7**	**9.8**	**10.0**	**10.0**
Sep	6.8	6.6	6.7	6.6	6.6	6.8	7.0
Oct	24.4	23.6	24.1	23.4	23.7	24.2	24.6
Nov	37.4	36.6	37.1	36.3	36.7	37.2	38.0
Dec	42.5	41.7	42.2	41.4	41.8	42.3	41.9
RMSD(°)	0.35	0.78	0.53	0.97	0.7	0.42	-

$$\mathrm{RMSD}(^\circ) = \left[\frac{1}{n}\sum_{i=1}^{n}\left(\beta_{opt,j,meas} - \beta_{opt,j,k}\right)^2\right]^{1/2}, \quad (11)$$

where $\beta_{opt,j,k}$ are the monthly optimum tilt angles using simulated monthly average daily diffuse horizontal irradiation data from the decomposition models, k = LJK, Page, CPR, Iqbal, Erbs *et al.*, or Ibrahim. So, for Table V, the *RMSDs* were calculated for all k when j = MI. The smaller the *RMSD*, the closer the match between $\beta_{opt,j,meas}$ and $\beta_{opt,j,k}$.

Figure 3(a) shows the *RMSDs* obtained from all six tables. First, it can be deduced that the LJK decomposition model is best suited to the local climate as its *RMSDs* are the smallest regardless of the transposition model used (by comparison, the Iqbal model is the least suitable). Still using the LJK model, the lowest *RMSD* was achieved when monthly optimum tilt angles were modeled by the MI transposition model, while the highest *RMSD* occurred for the B transposition model. In the ascending order of *RMSD*, the transposition models are arranged as MI, HDKR, K, HD, LJ, and B and this pattern is repeated for every other decomposition model with concomitant widening ranges of *RMSD* on the order of LJK, Ibrahim, CPR, Erbs *et al.*, and Page and Iqbal. Figure 3(b) specifies the *RMSD* values for all the transposition models using the LJK and Iqbal decomposition models as examples which highlight how decomposition model selection can significantly affect the accuracy of computed monthly optimum tilt angles. It should be obvious that if a decomposition model accurately predicts the measured monthly average daily diffuse horizontal irradiation, then the *RMSD* values for all the transposition models would be zero. Notice that the order of increasing *RMSD* is the same as the order of increasing deviation of the models from the reference tilt angles of the beam irradiation shown in Fig. 2 and Table IV. This indicates that the further away that a transposition model's tilt angles are from the reference angles, the greater its sensitivity to the changes in the isotropic diffuse irradiation component furnished by the decomposition models.

Although the preceding analyses may not allow one to pinpoint the best transposition model to apply to the local climate without experimental verification, the fact that (i) it is well documented and known that isotropic models, though simpler and more convenient to use, do not represent the realistic anisotropic nature of sky diffuse irradiation and (ii) the foregoing analyses have shown very good agreement among the anisotropic models leads this study to focus on the HD, HDKR, and MI models as most applicable to the local climate. Consequently, Table VI lists the top ten decomposition-transposition model matches obtained from Fig. 3(a) for which the *RMSD* is less than 1°. It is grouped by the transposition model and on the order of increasing *RMSD* shown in the parentheses.

The MI model can be paired with five decomposition models (LJK, Ibrahim, CPR, Erbs *et al.*, and Page). The HDKR model can be paired with three decomposition models (LJK, Ibrahim, and CPR). The HD model can be paired with two decomposition models (LJK and Ibrahim). Recall that the sensitivity of the anisotropic models to the isotropic component of the diffuse irradiation decreases as they get closer to the beam irradiation reference angles. Therefore, the MI model can tolerate the

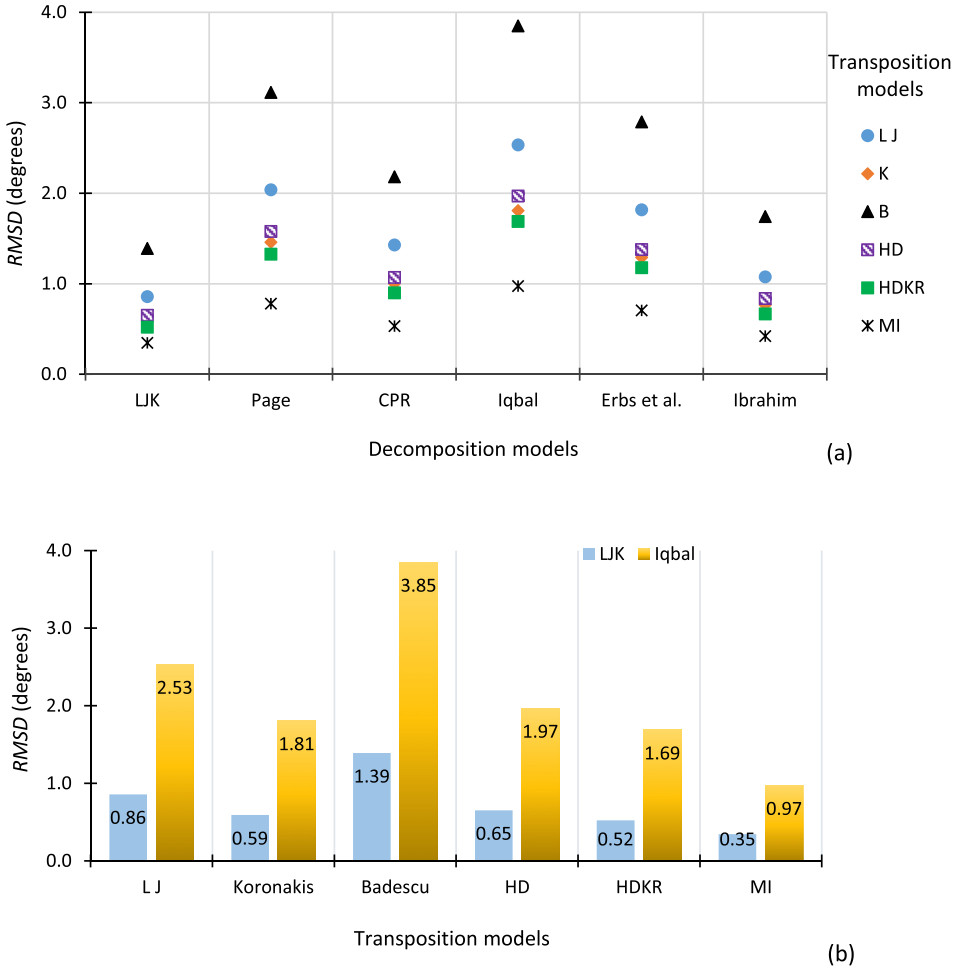

FIG. 3. (a) The *RMSD* between the monthly optimum tilt angles due to each of the decomposition models and those using the measured monthly average daily diffuse horizontal irradiation for each of the six transposition models and (b) the *RMSD* results from the LJK and Iqbal models.

TABLE VI. The top ten decomposition-transposition model matches for the HD, HDKR, and MI models with *RMSD* $< 1°$. The values of *RMSD* are shown in the parentheses.

Decomposition-transposition model matches	
LJK-MI (0.35°)	LJK-HDKR (0.52°)
Ibrahim-MI (0.42°)	Ibrahim-HDKR (0.67°)
CPR-MI (0.53°)	CPR-HDKR (0.90°)
Erbs *et al.*-MI (0.70°)	LJK-HD (0.65°)
Page-MI (0.78°)	Ibrahim-HD (0.84°)

predictive inaccuracies of the decomposition models proposed by Erbs *et al.* and Page. However, the HDKR model cannot, due to its greater sensitivity to the isotropic diffuse component, which is further exacerbated by the HD model.

Thus, if Trinidad did not possess measured diffuse horizontal irradiation data and a decision had been made to unbiasedly use any of the three anisotropic models to simulate tilted solar collectors, then the most suitable decomposition-transposition model matches are listed in Table VI which gives the assurance that the monthly optimum tilt angles would be within 1° RMSD of the actual values. Of course, the LJK decomposition model would be favored locally with either of the three anisotropic models.

Significantly, the information in Table VI can be used by territories which do not have any measured diffuse horizontal irradiation data but a similar climate to Trinidad. These decomposition-transposition model matches would allow for the best possible estimations of such territories' monthly optimum tilt angles and plane-of-array GSI, in the absence of the corresponding comparative empirical measurements. Now, it is conceivable that the ranking and the RMSD values (even while they remain less than 1°) may change in different territories due to slight differences in the clearness indices and the ratio of the beam to diffuse horizontal irradiation even while it remains greater than 1, for the average days of the months, as in this analysis of Trinidad (see Fig. 1). Hence, we are not concerned with identifying a single best decomposition-transposition model match based on its lowest RMSD as this can change with territory, but to present an applicable suite of matches which in this analysis produced values of RMSD $< 1°$ for the three

anisotropic models under consideration. The ten entries in Table VI were used for explicatory purposes, and territories are free to reduce that number. We recommend a reduction to a minimum of two decomposition models, LJK and Ibrahim.

This easily implementable decomposition-transposition model matching technique can be exported globally to any host territory having the requisite data to establish its own decomposition-transposition model matches for use by other territories possessing a similar climate to the host. In this way, a global network of host-to-user territories can be established, to the benefit of the solar energy community.

D. Detailed analysis of south/north and south-oriented flat-plate solar collectors

1. Selecting a transposition model to simulate the flat-plate solar collectors

Figure 4(a) shows the measured annual horizontal GSI and the values predicted by all the transposition models for a monthly optimized south/north collector, together with the percentage gains in the annual GSI of the tilted compared with the horizontal case. It is clear that the isotropic models predict smaller gains than the anisotropic models. The lowest and highest gains are modelled by the B and MI models, respectively. As intimated in Subsection IV C, the HD, HDKR, and MI models are the preferred models for the local climate. Rather than being conservative, we choose to use the MI model which predicts the highest annual tilted GSI of 6318 MJ m^{-2} for the ensuing detailed analysis, with the knowledge that this value may be approximately 1.1% lower as predicted by the HD model. This is shown in Fig. 4(b), which plots the percentage differences in the annual tilted GSI of the LJ, K, B, HD, and HDKR models relative to the chosen MI model.

2. Monthly, seasonal, and annual optimum tilt angles of the MI transposition model

Figures 5(a) and 5(b) show the monthly, seasonal, and annual optimum tilt angles for south/north-oriented and south-oriented collectors, respectively, together with a reference horizontal collector.

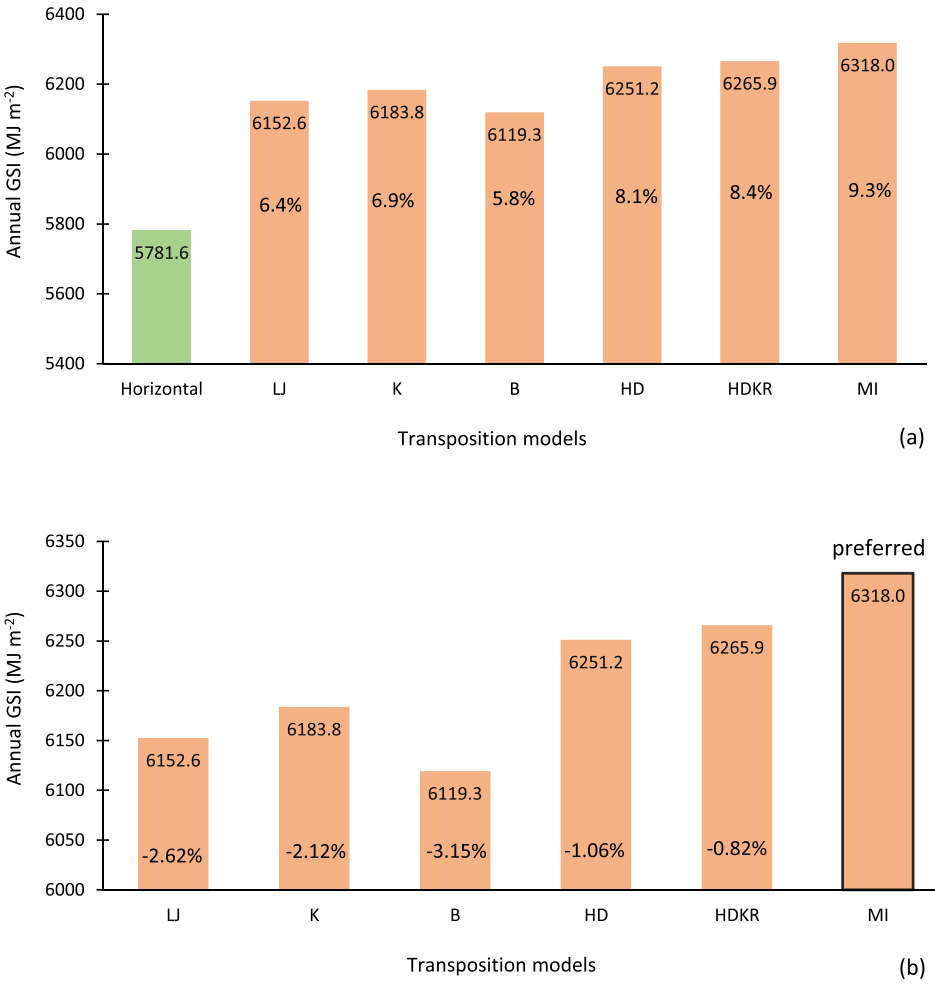

FIG. 4. Annual GSI predicted by the six transposition models for a monthly optimized tilted south/north-oriented solar collector along with (a) the measured horizontal irradiation and percentage gains in the annual GSI of the tilted over the horizontal collector and (b) the percentage differences in the annual GSI predicted by the LJ, K, B, HD, and HDKR models relative to the preferred MI model.

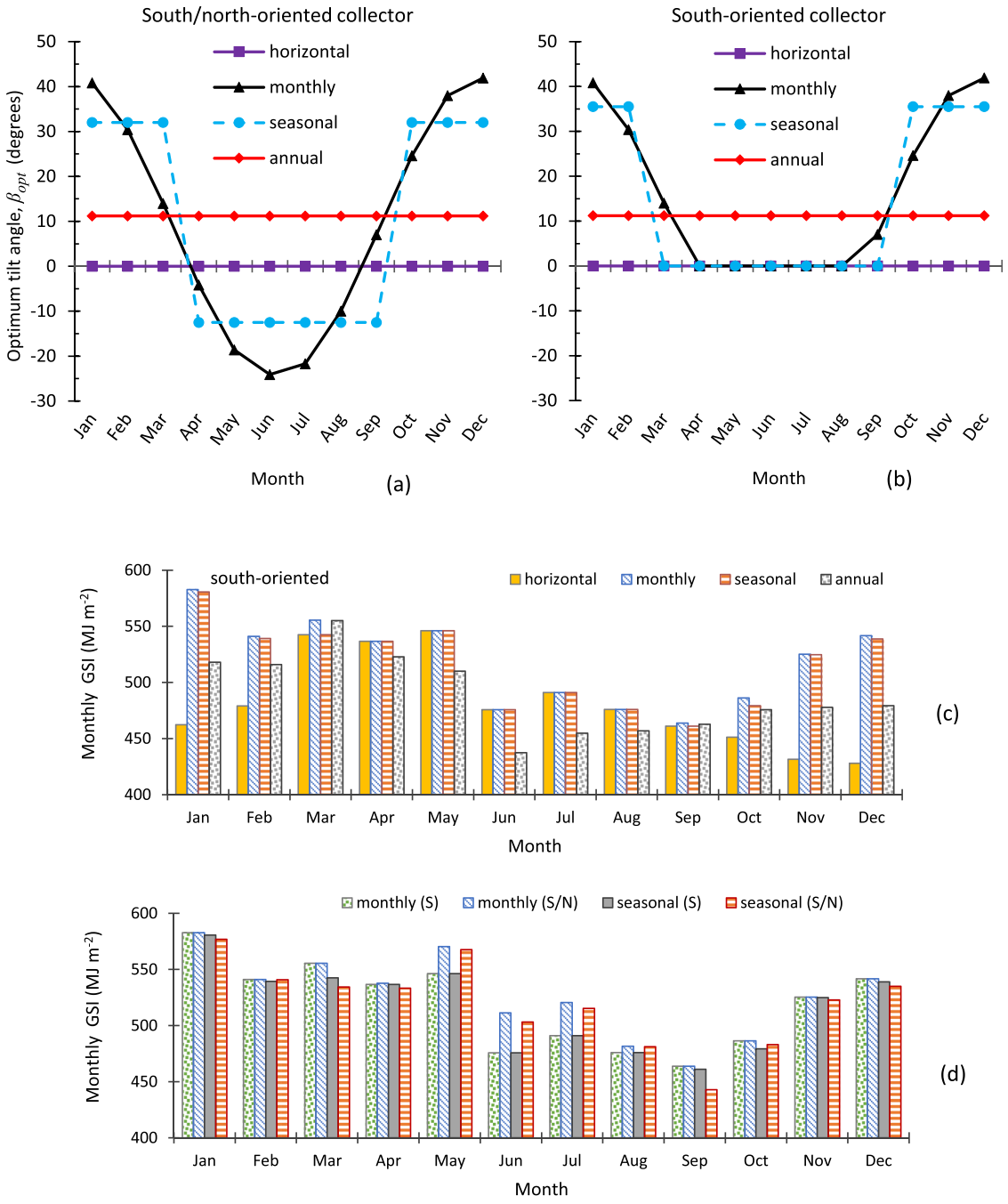

FIG. 5. Monthly, seasonal, and annual optimum tilt angles for (a) south/north-oriented and (b) south-oriented solar collectors modelled by the MI transposition model and the monthly GSI collected for (c) the south-oriented collector and (d) comparison of its monthly and seasonal performance with the south/north-oriented collector.

The monthly optimum tilt angle graphs differ only during the months of April to August. The south-oriented collector must be kept horizontal (β_{opt} = 0°) to collect the maximum GSI during these months, and as explained earlier, the south/north-oriented collector must be oriented north for these 5 months. It is also clear that a south/north-oriented collector requires 12 adjustments (every month) per year, while a south-oriented collector requires 8 adjustments (January–March, April, and September–December).

It is practically possible but may be undesirable to adjust the tilt angle of a collector 12 and 8 times per year, more so, if one is considering large solar collectors and/or large solar farms/photovoltaic plants where the cost for its implementation through personnel and operation (manual or automated) is considered. The aim is thus to minimize the number of adjustments required annually without compromising detrimentally the GSI collected annually. This was achieved by seasonally adjusting the tilt angles of the collectors twice per year as shown in Figs. 5(a) and 5(b). Seasonal adjustments occurred in April (12.5° north-oriented) and October (32° south-oriented) for the south/north-oriented collector and in March (0°) and October (35.5°) for the south-oriented collector. Designating their operations in terms of latitude, φ, a south/north-oriented surface should be tilted at approximately $(\varphi + 21^\circ)$ from October to March (south-oriented) and $(\varphi + 2^\circ)$ from April to September (north-oriented), while a south-oriented collector should be tilted at $(\varphi + 25^\circ)$ from October to February and 0° otherwise.

If an annual fixed-tilt collector is desired, then it should be oriented south at a tilt angle of 11.2°. It should be noted that this tilt angle supports the general rule-of-thumb recommendation that an annual fixed-tilt collector should be oriented southwards at a tilt angle equal to the latitude of the location for countries in the northern hemisphere. The value of 11.2° agrees well with the latitude (of the weather station) of approximately 10.6°N, exceeding it by 0.6°.

Table VII summarizes the aforementioned analysis with the details of the annual GSI collected, including the case for a fixed horizontal ($\beta = 0^\circ$) collector.

3. Annual and monthly GSI predicted by the MI transposition model

From Table VII, it is found that the horizontal collector harvests the lowest GSI annually. The annual GSI increases in order from annual, seasonal, and monthly tilted south-oriented collectors to seasonal and monthly tilted south/north-oriented collectors. Of significance is the fact that the annual GSI of the twice-adjusted seasonal south/north-oriented collector exceeds that of the monthly eight-times-adjusted south-oriented collector, which would amount to greater convenience and reduced operation and maintenance costs. The highest percentage gain possible is about 9.3% annually for monthly adjustments of the south/north-oriented collector. The gain falls by about 1.4%, yielding a value of 7.9% for just two seasonal adjustments per year.

Knowledge of the monthly GSI collected is also important for power-generating photovoltaic plants to assess monthly electrical power-generating capacity which along with historical monthly electrical-loading data would allow for better planning, design, and implementation.

Figure 5(c) shows the monthly GSI collected by a south-oriented collector operated in its three modes (monthly, seasonal, and annual) along with a reference horizontal setting. Figure 5(d) compares the monthly GSI collected by south-oriented (S) and south/north-oriented (S/N) collectors for the monthly and seasonal cases since these are the only cases that differ between an S and S/N collector.

The relative differences in the monthly GSI collected can be easily explained by making use of Figs. 5(a) and 5(b) and noting that (i) a monthly optimized collector maximizes the monthly GSI collected and consequently, (ii) the closer the seasonal, annual, and horizontal tilt angles are to the monthly optimum tilt angles, the higher their monthly collectable GSI will be.

For example, consider the month of January in Figs. 5(b) and 5(c). The seasonal tilt angle is the closest to the monthly tilt angle followed by the annual and horizontal tilt angles. Therefore, the GSI collected should decrease in the order of monthly, seasonal, annual, and horizontal as is evident in Fig. 5(c). Again, for April to August in Fig. 5(b), the monthly, seasonal, and horizontal tilt angles coincide, while the annual tilt angle does not, and hence, the GSI collected in Fig. 5(c) is equal for the

TABLE VII. Flat-plate solar collector in a horizontal position and its MI-predicted optimum tilt angles for adjustments made monthly, seasonally, and annually for south/north-oriented and south-oriented collectors. Emboldened angles are for a north-facing collector, otherwise south-facing. Annual GSI collected and percentage gains (in parentheses) of the tilted over the horizontal surface are shown.

Month	Horizontal (annually) β [°]	Monthly adjustments (12 annually) south/north β_{opt} [°]	Seasonal adjustments (Apr. and Oct.) south/north β_{opt} [°]	Monthly adjustments (8 annually) south β_{opt} [°]	Seasonal adjustments (Mar. and Oct.) south β_{opt} [°]	Annual (fixed tilt) south β_{opt} [°]
Jan	0	40.8	32	40.8	35.5	11.2
Feb		30.4	32	30.4	35.5	
Mar		14	32	14	0	
Apr		**4.2**	**12.5**	0	0	
May		**18.6**	**12.5**	0	0	
Jun		**24.1**	**12.5**	0	0	
Jul		**21.7**	**12.5**	0	0	
Aug		**10**	**12.5**	0	0	
Sep		7	**12.5**	7	0	
Oct		24.6	32	24.6	35.5	
Nov		38	32	38	35.5	
Dec		41.9	32	41.9	35.5	
Annual GSI (MJ m^{-2})	5781.6	6318.0 (9.3%)	6236.2 (7.9%)	6222.0 (7.6%)	6192.0 (7.1%)	5867.1 (1.5%)

monthly, seasonal, and horizontal cases but lower for the annual case. Similar analyses hold for all other months of the year. Also to be noted from Fig. 5(c) is that when compared to the horizontal case, January experiences the largest % gain in the collected GSI of 26% for monthly optimum tilt angles.

Now, consider Fig. 5(d) and the monthly adjusted collectors shown in the first two bars of every month. For April to August, the increase in monthly GSI is evident for the S/N surface when it is north-oriented. These months are responsible for the higher annual GSI recorded in Table VII since for all other months, the S and S/N surfaces collect equal GSI due to the same tilt angles and orientations as seen in Figs. 5(a) and 5(b). As previously done, the latter figures also explain the relative differences between the seasonally adjusted surfaces shown in the last two bars of every month in Fig. 5(d). For example, the S/N collector harvests more GSI from May to August, while it faces north [during April to September in Fig. 5(a)] compared to the S collector, due to its tilt angles being closer to the ideal monthly optimum tilt angles. All other months can be analyzed similarly, and the following general observations between the collectors can be made:

- The S/N collector harvests more annual GSI in monthly and seasonal modes and equal GSI in the annual mode (Table VII) compared to the S collector.
- Compared to the S collector, the S/N collector collects more GSI for 5 months (April to August) and equal GSI for the remaining 7 months for monthly adjustments; more GSI for 6 months (February, May–August, and October) and less GSI for the remaining 6 months for seasonal adjustments; and equal GSI for all months for annual adjustments.
- For monthly and seasonal modes, both the S/N and S collectors harness maximum and minimum GSI in January and September, respectively, while for the annual mode, they collect maximum and minimum GSI in March and June, respectively.

The detailed simulations and analyses of the S/N and S collectors using the MI model have been completed.

Finally, it is prudent and instructive to briefly compare all the transposition models with regard to their annual GSI and percentage gains over the measured horizontal GSI, together with the five unchosen models' percentage differences in the annual GSI relative to the chosen MI model. Table VIII provides that information for all modes of operation of the flat-plate collectors/panels. The first row in Table VIII for the S/N monthly optimized collector is familiar to the reader and is plotted in Figs. 4(a) and 4(b) which themselves reflect a general behavior exhibited in the four remaining operational modes of the collectors in Table VIII.

V. CONCLUSION

Six transposition models comprising three isotropic models due to Liu and Jordan, Koronakis, and Badescu, and three anisotropic models due to Hay and Davies, "Hay and Davies, Klucher and Reindl," and Ma and Iqbal were evaluated for modeling the monthly optimum tilt angles of a flat-plate solar collector capable of south or north orientations, in the Caribbean island of Trinidad. The models used measured the monthly average daily global and diffuse horizontal irradiation inputs from the six-year period 2005–2010. The sky conditions for typical days of every month of the year were classified as intermediate or partly cloudy with a monthly average daily clearness index range of 0.41–0.5. The anisotropic models showed close agreement with one another and with computed reference monthly optimum tilt angles for the beam irradiation only, while the Liu and Jordan and Badescu models were skewed away from these reference angles. A decomposition-transposition model matching technique was developed which utilized six existing decomposition models (Liu and Jordan and Klein, Page, Collares-Perreira and Rabl, Iqbal, Erbs *et al.*, and Ibrahim) to simulate the monthly average daily diffuse horizontal irradiation, and the corresponding monthly optimum tilt angles for the six transposition models were computed. The most suitable decomposition-transposition model matches were determined which can be used by territories having a similar climate to Trinidad but where measured

TABLE VIII. The transposition models' predicted annual GSI, % gains over the measured horizontal GSI, and the horizontal, LJ, K, B, HD, and HDKR's % differences relative to the chosen MI model, for the five operational modes of the solar collector/panel.

Solar collector's operational mode	Annual GSI, % gains, and % differences	Horizontal	LJ	K	B	HD	HDKR	MI
S/N: monthly optimized	Annual GSI (MJ m^{-2})	5781.6	6152.6	6183.8	6119.3	6251.2	6265.9	6318.0
	% gain over horizontal	…	6.42	6.94	5.84	8.12	8.38	9.28
	% difference relative to MI	−8.49	−2.62	−2.12	−3.15	−1.06	−0.82	…
S/N: seasonally optimized	Annual GSI (MJ m^{-2})	5781.6	6093.3	6121.9	6061.0	6178.3	6188.7	6236.2
	% gain over horizontal	…	5.39	5.89	4.83	6.86	7.04	7.86
	% difference relative to MI	−7.20	−2.26	−1.81	−2.77	−0.92	−0.75	…
S:monthly optimized	Annual GSI (MJ m^{-2})	5781.6	6086.9	6111.7	6061.0	6167.5	6180.2	6222.0
	% gain over horizontal	…	5.28	5.71	4.83	6.68	6.89	7.62
	% difference relative to MI	−7.08	−2.17	−1.77	−2.59	−0.87	−0.67	…
S: seasonally optimized	Annual GSI (MJ m^{-2})	5781.6	6066.5	6090.0	6041.5	6141.8	6153.8	6192.0
	% gain over horizontal	…	4.93	5.33	4.49	6.23	6.44	7.10
	% difference relative to MI	−6.60	−2.02	−1.64	−2.42	−0.81	−0.61	…
S:fixed tilt	Annual GSI (MJ m^{-2})	5781.6	5839.3	5845.6	5831.9	5856.1	5857.2	5867.1
	% gain over horizontal	…	1.00	1.11	0.87	1.29	1.31	1.48
	% difference relative to MI	−1.35	−0.44	−0.34	−0.56	−0.17	−0.16	…

diffuse horizontal irradiation and validating tilt angles or plane-of-array measurements do not exist, thereby eliminating ad-hoc selection of decomposition and transposition models for simulation purposes. The technique can be exported globally to improve the accuracy of simulations of tilted solar collectors/panels. The Ma and Iqbal model was selected to model the foregoing collector as well as the one that was south-oriented only, at a latitude of $\varphi = 10.6^\circ$ N. A south/north-oriented collector required twelve monthly, two seasonal [April: $\varphi + 2^\circ$ (north-oriented) and October: $\varphi + 21^\circ$ (south-oriented)], and annual [January: $\varphi + 0.6^\circ$ (south-oriented)] adjustments with the corresponding gains in the annual global solar irradiation collected compared to that on a horizontal surface of 9.3%, 7.9%, and 1.5%, respectively. In contrast, a south-oriented collector required eight monthly (September–April) and two seasonal (March: 0° and October: $\varphi + 25^\circ$) adjustments with lower corresponding gains in annual global solar irradiation of 7.6% and 7.1%, respectively. This study provides an easily implementable decomposition-transposition matching technique with global application, useful insights and perspectives, and a new "data point" to the international solar energy community at a latitude with a tropical maritime and modified moist equatorial climate which is also invaluable for planners, designers, and investors in photovoltaic systems in Trinidad.

ACKNOWLEDGMENTS

The author recognizes the invaluable contribution of the Trinidad and Tobago Meteorological Service for providing the data used in this study and the support at the Center for Optoelectronics Research.

REFERENCES

[1]D. Yang, Sol. Energy **136**, 288 (2016).
[2]B. Y. H. Liu and R. C. Jordan, Sol. Energy **4**, 1 (1960).
[3]S. A. Klein, Sol. Energy **19**, 325 (1977).
[4]J. K. Page, in *Proceedings of UN Conference on New Sources of Energy* (1961) (1961), p. 378.
[5]M. Collares-Pereira and A. Rabl, Sol. Energy **22**, 155 (1979).
[6]M. Iqbal, Sol. Energy **24**, 491 (1980).
[7]D. G. Erbs, S. A. Klein, and J. A. Duffie, Sol. Energy **28**, 293 (1982).
[8]S. M. Ibrahim, Energy Convers. Manage. **25**, 69 (1985).
[9]N. Al-Rousan, N. Isa, and M. Desa, Renewable Sustainable Energy Rev. **82**, 2548 (2018).
[10]B. Y. H. Liu and R. C. Jordan, ASHRAE Trans. **67**, 526 (1961).
[11]P. S. Koronakis, Sol. Energy **36**, 217 (1986).
[12]V. Badescu, Renewable Energy **26**, 221 (2002).
[13]J. E. Hay and J. A. Davies, in *Proceedings of the First Canadian Solar Radiation Data Workshop*, edited by J. E. Hay and T. K. Won (Ministry of Supply and Services, Toronto, Canada, 1980), p. 59.
[14]D. T. Reindl, W. A. Beckman, and J. A. Duffie, Sol. Energy **45**, 9 (1990).
[15]J. A. Duffie and W. A. Beckman, *Solar Engineering of Thermal Processes* (John Wiley & Sons, New York, 2013).
[16]C. Ma and M. Iqbal, Sol. Energy **31**, 313 (1983).
[17]T. M. Klucher, Sol. Energy **23**, 111 (1979).
[18]P. I.Cooper, Sol. Energy **12**, 3 (1969).
[19]Z. Sen, Sol. Energy **63**, 39 (1998).
[20]B. Y. H. Liu and R. C. Jordan, Sol. Energy **7**, 53 (1963).
[21]K. De Souza, J. Renewable Sustainable Energy **10**, 043703 (2018).
[22]M. Alves, L. Sanches, J. Nogueria, and V. Silva, Atmos. Clim. Sci. **3, 618** (2013).
[23]D. H. W. Li, C. C. S. Lau, and J. C. Lam, Build. Environ. **39**, 101 (2004).
[24]A. Kuye and S. S. Jagtap, Sol. Energy **49**, 139 (1992).